MethodsX 14 (2025) 103410

Contents lists available at ScienceDirect

MethodsX

journal homepage: www.elsevier.com/locate/methodsx

Automated detection of epicardial adipose tissue in cardiac CT using ensemble machine learning for improved diagnosis

Jasmine S*, Marichamy P

Department of Electronics and Communication Engineering, P.S.R Engineering College, Sivakasi, Tamilnadu, India, 626140

ARTICLE INFO

Method name:
Automated Detection of Epicardial Adipose Tissue using Ensemble Machine Learning (SVM + ANN)

Keywords:
Machine learning
Epicardial fat
Adipose tissue segmentation
Cardiovascular risk
Medical imaging
Computed tomography

ABSTRACT

Cardiovascular diseases remain a major global health concern, with epicardial adipose tissue (EAT) serving as a critical indicator for assessing cardiovascular risk. Performing manual delineation of epicardial adipose tissue (EAT) on cardiac CT scans is a labour-intensive process and can be susceptible to inaccuracies. This study presents an automated machine learning-based approach to improve the accuracy and efficiency of EAT segmentation. A dataset of 878 cardiac CT images from 20 patients is used. Pre-processing involved contrast enhancement and feature extraction using the Grey-Level Co-occurrence Matrix (GLCM). An ensemble machine learning model combining Support Vector Machine (SVM) and Artificial Neural Network (ANN) is developed for segmentation. The model's performance was evaluated using accuracy, precision, recall, Dice score, and classification time. The key highlights of the proposed method are:

- **Automated EAT segmentation** using a hybrid ensemble approach (SVM + ANN).
- **Feature extraction with GLCM** enhances segmentation accuracy.
- **Improved performance** over traditional methods, reducing processing time and increasing precision.

This method offers a promising solution for automated EAT detection, enabling efficient cardiovascular risk assessment.

Specifications table

Subject area:	Computer Science
More specific subject area:	Machine Learning for Epicardial Adipose Tissue (EAT) Segmentation in Cardiac CT
Name of your method:	Automated Detection of Epicardial Adipose Tissue using Ensemble Machine Learning (SVM + ANN)
Name and reference of original method:	EAT Segmentation using Machine Learning. **Reference:** É. O. Rodrigues, V. H. A. Pinheiro, P. Liatsis, and A. Conci, "Machine learning in the prediction of cardiac epicardial and mediastinal fat volumes," Comput. Biol. Med., 2017, 89, 520–529. https://doi.org/10.1016/j.compbiomed.2017.02.010
Resource availability:	**Dataset:** *https://visual.ic.uff.br/en/cardio/ctfat/* ***Software:*** Python (Scikit-learn, TensorFlow/Keras) **Hardware:** NVIDIA RTX A2000 GPU

* Corresponding author.
E-mail addresses: sjasmine151098@gmail.com (J. S), pmarichamy@psr.edu.in (M. P).

https://doi.org/10.1016/j.mex.2025.103410
Received 27 March 2025; Accepted 30 May 2025
Available online 31 May 2025

Background

Cardiovascular diseases arise from various factors such as obesity, diabetes, aging, and hypertension. Epicardial adipose tissue (EAT), located between the heart muscle and the outer layer of the heart, is recognized as an important factor in coronary artery disease progression [1–5]. An excessive build-up of EAT has been linked to major heart-related disorders such as heart attacks [6], irregular heart rhythms [7], arterial rigidity [8], and hardening of the arteries [9–11]. The growth of visceral adipose tissue (VAT) alongside EAT can lead to systemic inflammation and metabolic disturbances, increasing the risk of cardiovascular events [12–16]. Moreover, EAT volume has been correlated with coronary artery calcification, a key predictor of cardiovascular events and certain cancers [17,18]. Population studies have further highlighted a high incidence of sudden cardiac deaths linked to these risk factors [19,20]. To assess adipose tissue structures, various imaging approaches including ultrasound, CT scans, and MRI are employed, with CT being preferred due to its high spatial resolution [21–25]. Nonetheless, delineation of EAT through manual or semi-automatic methods on CT images tends to be labor-intensive and inconsistent, highlighting the importance of developing fully automated and accurate segmentation techniques [26–29].

Earlier methods for EAT segmentation showed limited success. A semi-automated approach with pericardium identification achieved only 10 % accuracy (4/40 images) [30]. A thresholding-based method using Otsu's technique and the HARTA program improved accuracy to 98.83 % with a Dice score of 77.30 % [31]. AI-based techniques have since gained traction for cardiac fat segmentation, quantification, and diagnosis [32–34]. Larger datasets help reduce overfitting [35,36], and multi-atlas segmentation has lowered failure rates to 3 % [37]. Random Forest models reached 98.4 % accuracy but required 1881 s per image, later optimized to 163 s using atlas-based methods [29,38]. Rotation Forest with MLP halved processing time [39], and genetic algorithms (GA) further reduced the processing time [40]. J48Graft achieved 99 % accuracy in 132.86 s, while Naïve Bayes was faster (55.48 s) but less accurate (86 %) [41]. The Floor of Log (FoL) clustering method reduced segmentation time to just 2.01 s, with 93.45 % accuracy and 95.52 % specificity [42]. Gabor filter and texture-based segmentation yielded 99.2 % accuracy within 1 min [43]. Modified region-growing methods achieved Dice scores up to 98.7 % and high accuracy for both epicardial and mediastinal fat [44], while fuzzy affinity-based methods showed a mean sensitivity of 85.63 % ± 7.42 % [45].

Deep learning has recently dominated EAT segmentation. Dual U-Nets with morphological processing layers [46] improved boundary accuracy but required large datasets and high computation. Pix2Pix-conditional generative adversarial network [47] achieved high accuracy (98.33 %) and Dice score (98.73 %) with fast processing (1.44 s), but lacked interpretability. Attention-based BMT-UNet [48] enhanced fat quantification at the cost of increased model complexity. U-Net models [49] for low-dose CT struggled to balance accuracy and speed. Similarly, recent architectures like Dynamic RU-Next [50] and MNR^{2}NeXt [51] offer enhanced segmentation capabilities but demand significant computational resources.

Based on the analysis of existing methods, it is inferred that most approaches struggle to balance segmentation accuracy with processing time, limiting their clinical applicability. Classical machine learning (ML) techniques like Random Forest [38] and clustering algorithms such as Floor of Log (FoL) [42] have shown reasonable accuracy but often involve high computational costs or reduced precision. Although deep learning models like dual U-Nets [46], Pix2Pix GAN [47], and BMT-UNet [48] achieve high Dice scores, their performance is often dependent on extensive labeled training data and high-end computing capabilities.

To address these challenges, the current work introduces a novel ensemble-learning strategy that systematically evaluates ten SVM-based combinations with diverse classifiers, including Random Forest, CatBoost, XGBoost, LightGBM, K-Nearest Neighbors, Generalized Linear Model, RepTree, Artificial Neural Network, and hybrid variants. This novel approach uses the complementary strengths of these classifiers through a soft voting mechanism, which integrates their outputs to improve classification stability and segmentation performance. Additionally, the method incorporates Grey-Level Co-occurrence Matrix (GLCM) texture attributes to enhance differentiation between fat and non-fat tissue regions. By combining texture features with ensemble learning, the framework offers an efficient and practical solution for automated epicardial fat segmentation.

Method details

The proposed method follows a structured workflow consisting of data preprocessing, texture attribute extraction utilizing the GLCM, and classified segmentation through an ensemble-based machine learning framework. The core innovation lies in combining Support Vector Machine (SVM) with ten different classifiers using a soft voting mechanism to improve segmentation accuracy and model robustness. This ensemble is designed to exploit the strengths of both linear and nonlinear classifiers for effective classification of EAT from input images. Among the combinations evaluated, the hybrid SVM–ANN model delivered the highest segmentation performance and computational efficiency. Therefore, the detailed methodological discussion in this study focuses primarily on the SVM–ANN framework.

Dataset

A cardiac CT dataset provided by O. Rodrigues et al. [29], has been considered for the study. This dataset has 878 cardiac CT scan images of 20 different patients and their details are indicated in Table 1. All the data images were rescaled to −200 to −30 Hounsfield units (HU) for better visualization of the heart fat. These images are color-coded to distinguish between the different kinds of fats. Red pixels indicate epicardial fat, whereas green pixels show mediastinal fat. Notably, the dataset provides expert-annotated ground truth (GT) images and includes image registration as part of the preprocessing, making it well-suited and readily usable for both training and evaluation purposes.

Table 1
Patient demographics of the dataset.

Details	No.of patients	Mean age	No.of slices per Image
Men	11	55.4	42
Women	9	53	43.9

Evaluation metrics

This subsection outlines key metrics for assessing machine learning model performance: accuracy, recall, Dice score, and precision. These metrics are derived from a confusion matrix with true positives (TP), false positives (FP), true negatives (TN), and false negatives (FN). Precision assesses the correctness of positive identifications, while recall quantifies the ability to identify all positive instances in the dataset. The Dice similarity co-efficient (DSC) balances precision and recall by providing a harmonic mean, ensuring neither metric is overlooked, especially in imbalanced datasets. Lastly, accuracy measures ratio of correct predictions, encompassing both true positives and true negatives, thereby providing a comprehensive evaluation of the model's effectiveness in accurately segmenting EAT.

$$\text{Precision} = \frac{TP}{TP + FP} \tag{1}$$

$$Recall = \frac{TP}{TP + FN} \tag{2}$$

$$DSC = \frac{2 \times (Recall \times Precision)}{Recall + Precision} \tag{3}$$

$$Accuracy = \frac{TP + TN}{TP + TN + FP + FN} \tag{4}$$

Pre-Processing and GLCM feature extraction

The proposed method employs preprocessed cardiac CT images in BMP format, originally converted from DICOM and spatially registered by the dataset authors [29]. As all registration steps were completed in advance, no additional alignment is required. Fat masks were then generated by thresholding to separate fat from non-fat regions. For texture analysis, features were extracted using the Grey-Level Co-occurrence Matrix (GLCM), a statistical method that evaluates spatial relationships between pixel intensities. Four GLCM-based features were computed: energy, entropy, contrast, and correlation. Energy (Eq. (5)) reflects texture uniformity, with higher values indicating more homogeneity. Entropy (Eq. (6)) measures randomness, with greater values representing more complex textures. Contrast (Eq. (7)) captures intensity differences between neighbouring pixels, aiding edge detection. Correlation (Eq. (8)) assesses the linear relationship between pixel intensities, revealing structural patterns. In these equations, $F(a, b)$ denotes the normalized co-occurrence probability between gray levels a and b, while μ and σ represent the mean and standard deviation of gray levels, respectively.

$$Energy = \sum_{a,b} F(a, b)^2 \tag{5}$$

$$Entropy = \sum_{a,b} F(a, b) \log (F(a, b)) \tag{6}$$

$$Contrast = \sum_{a,b=0}^{N-1} Fa, b(a - b)^2 \tag{7}$$

$$Correlation = \sum_{a,b=0}^{N-1} Fa, b \left[\frac{(a - \mu a)(b - \mu b)}{\sqrt{(\sigma a^2)\ (\sigma b^2)}} \right] \tag{8}$$

Classified segmentation using ensemble combinations of SVM

In classified segmentation, a machine learning algorithm identifies whether a pixel in a cardiac CT image represents fat (white) or non-fat tissue (black) using feature vectors. This study evaluates SVM combined with ten algorithms: LightGBM, GBM, XGBoost, CatBoost, GLM, RepTree, KNN, Random Forest, ANN, and a Random Forest-CatBoost combination. Fig. 1 demonstrates classified segmentation using SVM and these algorithms. The machine learning frameworks for SVM-ANN ensembles are detailed in subsequent sections.

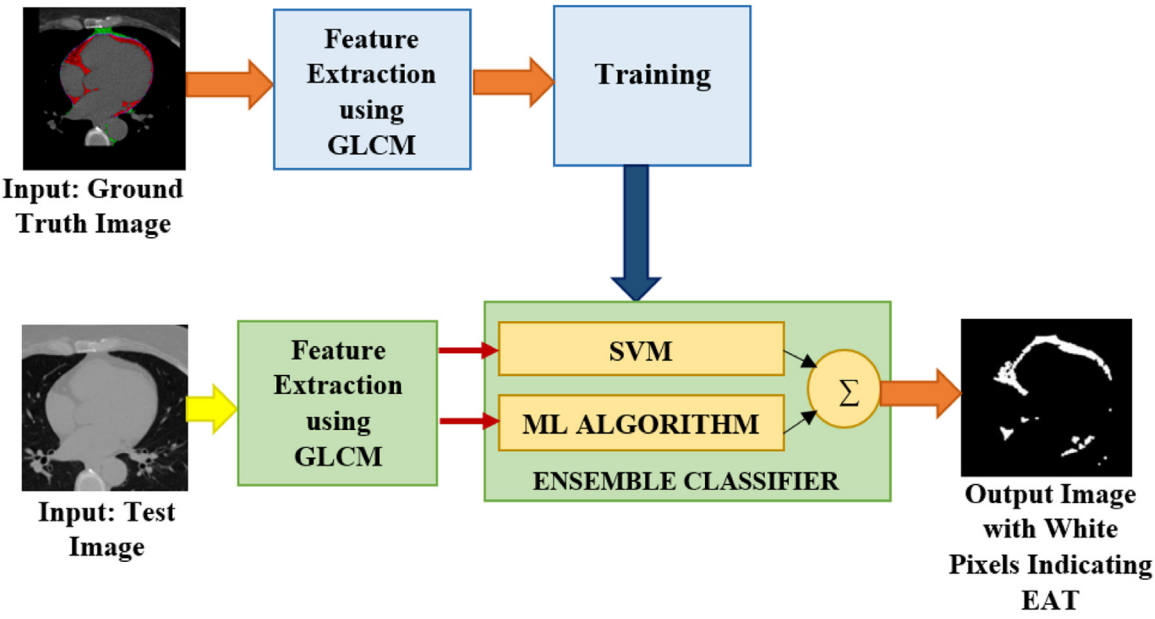

Fig. 1. Depiction of the classified segmentation process, which takes a cardiac CT image in DICOM format as input and yields a binary representation as output.

Support vector machine

SVM is a method for supervised ML. specifically developed for accurate estimation and classification tasks. Its robustness and adaptability make it well-suited for epicardial fat segmentation. Consider a linearly separable data set$\{a_i, b_i\}, i = 1, \ldots \ldots, N,\ b_i \in \{-1, +1\},\ a_i \in R^d$. In a space with d dimensions, the linear classification function which is employed as a hyperplane is expressed as:

$$w.a + c = 0 \tag{9}$$

To ensure efficient dataset separation, the classification threshold vector 'b' is optimized to enable the classifier to reliably distinguish all samples.

$$b_i\left(W \times a_i + C\right) - 1 \geq 0, i = 1, 2 \ldots ., n. \tag{10}$$

The optimal categorization plane is a hyperplane that maximizes the classification margin and satisfies criteria (10) and (11), as shown in Fig. 2. Eq. (11) and (12) represents the expression for the function objective and the most optimal classification.

$$\varphi = \min_{w,C} \frac{1}{2}\|w\|^2 = \frac{1}{2}(W \cdot w) \tag{11}$$

$$f(X) = sgn((W \times a) + C) = sgn\left(\sum_{i=1}^{N} A_i\ b_i\left(a_i \cdot X\right) + C\right) \tag{12}$$

In scenarios where linear separability is not possible, then Eqs. (11) and (12) can be solved with the inclusion of a relaxation variable and another penalty function. As a result, the solution to the issue is rewritten as the minimization of Eq. (13), where the parameter 'K' represents the penalty and is considered as a constant.

$$\varphi(W, \xi) = \frac{1}{2}(W.w) + K\left(\sum_{i=1}^{n} \xi_i\right) \tag{13}$$

Artificial neural networks (ANN)

Drawing inspiration from the biological neuron, ANNs comprise of interconnected neurons, arranged in layers called perceptrons. The MLP is a highly effective ANN structure with a feed-forward topology, typically trained using backpropagation and Levenberg-Marquardt optimization. As illustrated in Fig. 3, the MLP architecture is composed of three main layers: an input layer, one or more hidden layers, and an output layer.

The size of the input stage is determined by the dimensionality of the input data. Consider a vector x that has p input variables, represented as $x = [x_{1,} x_{2,\ldots\ldots,} x_p]^T$. In a neural network architecture designed for binary classification, the weight matrix is $W = [W_{ij}]$,

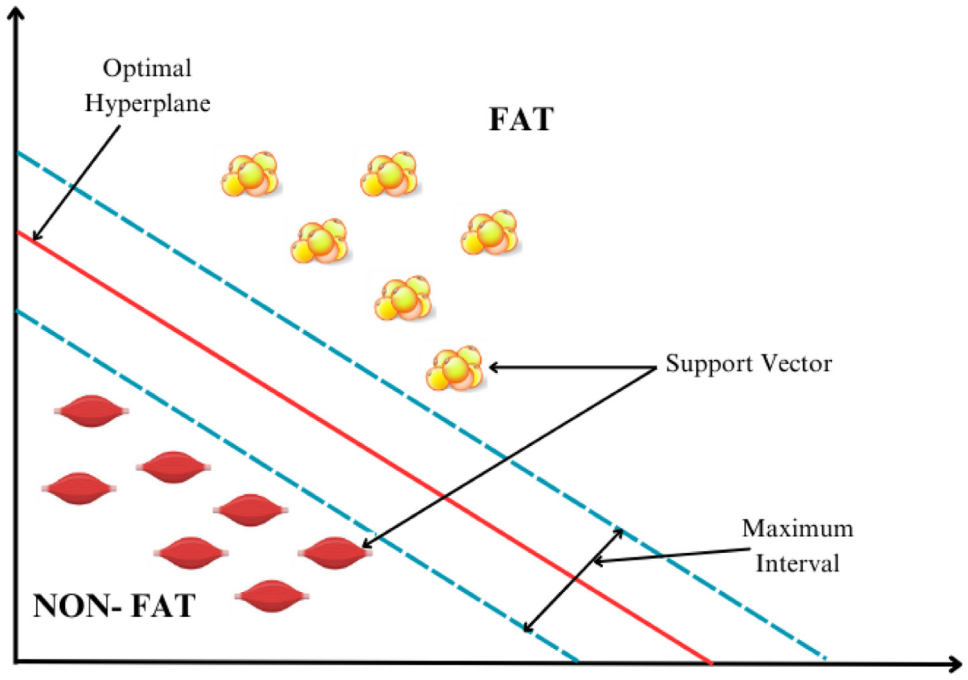

Fig. 2. Classification model of the support vector machine.

and the dimension $p \times q$ connects the p inputs to the q hidden layer nodes. Additionally, the vector $\upsilon = [\upsilon_1^h, \upsilon_{2,\ldots,}^h \upsilon_q^h]$ denotes the biases associated with the nodes in the hidden layer. Similarly, The weights connecting the q nodes in the hidden layer to only one output neuron are encapsulated inside the vector $k = [k_1^o, k_{2,\ldots,}^o k_q^o]$. As a result, the connection between input and output in the Multi-Layer Perceptron (MLP) designed for binary classification may be clearly expressed as:

$$y = \sigma\left(\sum_{j=1}^{q} k_j^o f\left(\left(\sum_{i=1}^{p} w_{ij} x_i\right) + \upsilon_j^h\right) + \upsilon^o\right) \tag{14}$$

In the given equation, $\sigma()$ denotes the sigmoid-based activation method, which limits the result to the interval [0, 1], making it appropriate for binary classification tasks. Meanwhile, f() indicates the activation mechanism employed in the hidden layer.

Integration of SVM and ANN

Voting classifiers are combined modelling approaches aimed at boosting predictive accuracy by integrating the outputs of multiple ML models. Among them, soft voting uses the probabilistic outputs of classifiers. Each classifier assigns probabilities to possible outcomes, and the class with the highest average probability across classifiers is selected. Fig. 4 illustrates the soft voting mechanism. In this study, we implemented a soft voting strategy to integrate SVM and MLP. SVMs are effective for separating classes in high-dimensional spaces but may struggle with nonlinear boundaries. In contrast, Multilayer Perceptrons (MLPs), a class of ANN, capture nonlinear dependencies efficiently. By combining both classifiers in a soft voting ensemble, the proposed model benefits from the geometric interpretability of SVM and the nonlinear adaptability of ANN, which is especially beneficial for segmenting epicardial fat. Table 2 provides pseudocode for the proposed ensemble learning approach.

Experimental setup, training details, and hyperparameter tuning

Experiments were conducted on an NVIDIA RTX A2000 GPU with an Intel Core i9 processor using the Cardiac CT Fat Dataset with 878 images. The dataset was split into 80 % training and 20 % testing. The method has been simulated, trained, and tested using the Python programming language. A manual hyperparameter tuning process was performed to optimize the SVM + ANN ensemble for epicardial fat segmentation. The tuning focused on SVM regularization parameter (C), gamma, kernel type, MLP hidden layer size, activation function, and maximum iterations. The experiments were conducted on images of size 128 × 128, with the accuracy varying across different configurations. The best accuracy of 98.57 % was achieved using $C = 0.1$, gamma = 10, RBF kernel, 100 hidden layers, ReLU activation, and 300 maximum iterations. These optimized hyperparameters significantly improved segmentation performance.

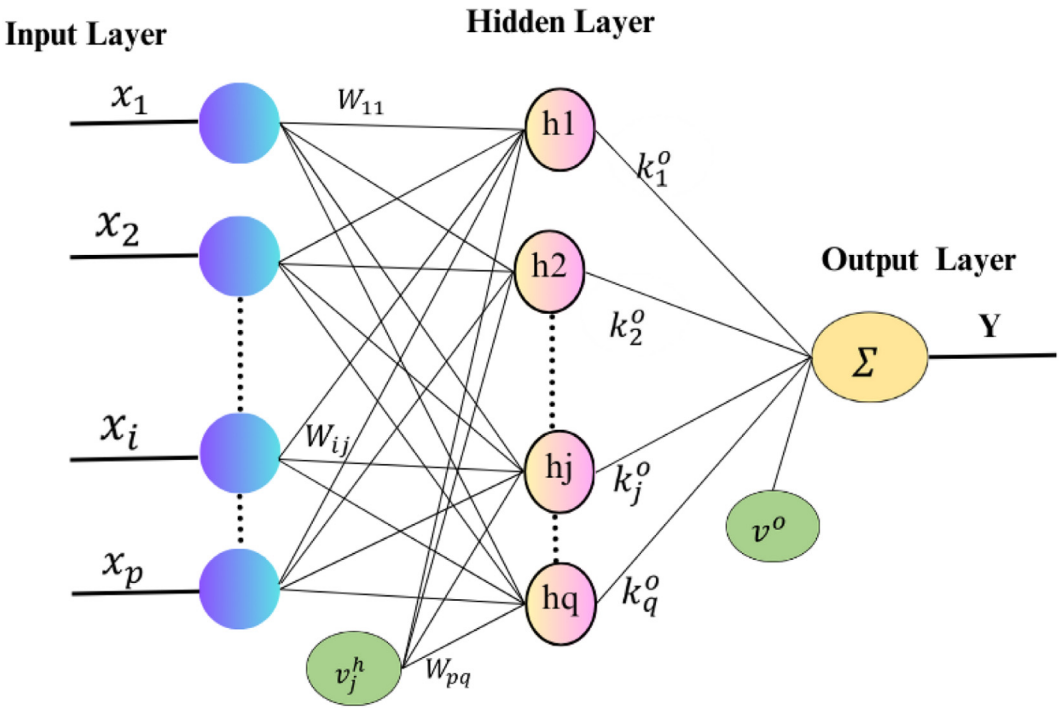

Fig. 3. Schematic representation of MLP.

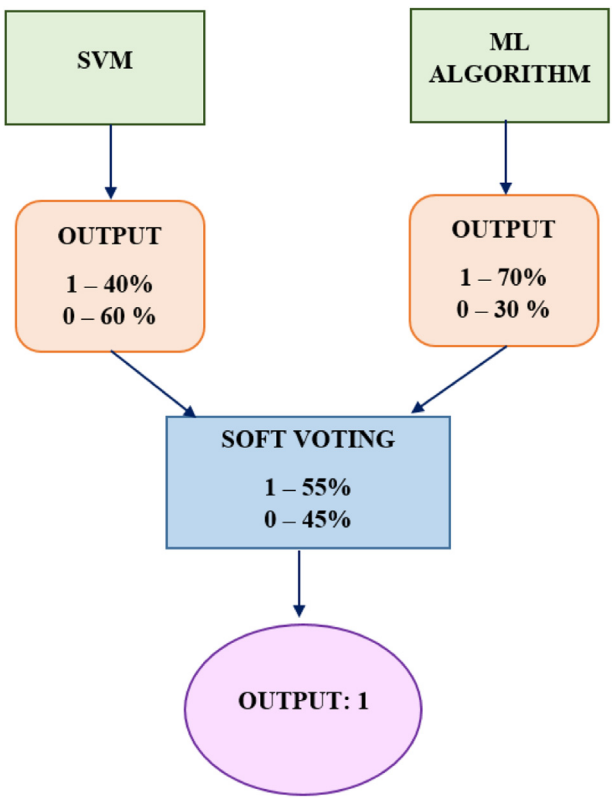

Fig. 4. Illustration of soft voting in ensemble machine learning techniques.

Table 2
Pseudo code for ensemble ML using soft voting.

Algorithm: ENSEMBLE COMBINATION OF SVM WITH ANN
Procedure SPLITTING_DATASET *(EAT_dataset)*
Training_data, Testing_data = assign (EAT_features,EAT_labels)
return *Training_data, Testing_dataVoting*_technique = "soft"
ML1 = *SVM (Training_data, labeled_ Groundtruth, Testing_data)*
ML2 = ANN (*Training_data, labeled_ Groundtruth, Testing_data)*
Procedure Ensemble_Technique (*Training_data, labeled_ Groundtruth, Test_samples)*
softvoting_classifier = concatenate (ML1, ML2)
softvoting_classifier.fit (*X=Train_samples, Y=Groundtruth_labels)*
SVM_ANNclassification = soft_voting_classification.classify(Test_samples)

Table 3
Performance of various ensemble models associated with the SVM.

Ensemble Combinations of SVM	Accuracy (%)	Precision (%)	Recall (%)	DSC (%)
SVM	94.20	94.30	94.10	94.20
SVM + RepTree	96.69	96.80	96.70	96.75
SVM + LightGBM	96.95	97.00	96.90	96.95
SVM + Gradient Boosting Machine (GBM)	96.95	97.10	97.00	97.05
SVM+ *K*-Nearest Neighbors (KNN)	97	97.50	97.13	97.31
SVM + Generalized Linear Model (GLM)	97.05	97.39	97.24	97.31
SVM + Xgboost	97.06	97.56	97.37	97.46
SVM + CatBoost (CB)	97.085	97.59	97.48	97.53
SVM + RandomForest +CatBoost	97.84	97.62	97.62	97.62
SVM + RandomForest (RF)	98.13	97.70	97.70	97.70
SVM+ANN(MLP)	**98.57**	**98.00**	**98.00**	**98.00**

Table 4
Comparison of epicardial fat segmentation techniques using CT images.

Authors & Year	Algorithm	Performance		Classification Time (Seconds)
		Accuracy (%)	DSC (%)	
Barbosa et al., & 2011	Cubic interpolation [30]	52.5	–	–
Shahzad et al., & 2013	Multi-Atlas [37]	-	89.15	–
Zhang et al., & 2020	Dual U-Nets [46]	–	91.19 ± 1.4	–
Rodrigues et al., & 2015	Random Forest [38]	98.4	96	1881
Rodrigues et al., & 2016	Atlas approach with Random Forest [29]	98.5	98.1	163
Rodrigues et al., & 2017	Random Forest+MLP [39]	98.5	–	81.5
Kazemi et al., & 2021	Gabor Filter [43]	99.2	98.03	60
Rodrigues et al., & 2017	GA [40]	–	–	54
Rebelo et al., & 2022	Thresholding [31]	98.83	77.30	15.5 ± 2.42
Priya and Sudha & 2019	Adaptive Fruitfly [44]	98.76	98.71	7.5
Liu et al., & 2023	3D U-Net [49]	–	70.97	6
Albuquerque et al., & 2020	Clustering [42]	93.45	–	2.01
Santos da Silva et al., & 2024	Pix2Pix Network [47]	98.33	98.73	1.44
Wang et al., & 2025	BMT-U Net [48]	98.30	–	1.43
Proposed	SVM –ANN Ensemble	98.57	98	1.40

*Entries are ordered from slowest to fastest reported processing times in the literature.

Method validation

This section compares the SVM+ANN ensemble with nine novel SVM-based ensembles to demonstrate its efficiency in EAT segmentation. The performance is also evaluated against existing methods to highlight its accuracy and robustness.

Performance of different ensemble combinations of SVM

To assess the performance of ensemble ML algorithms for epicardial fat segmentation, the results of a stand-alone SVM were first examined, which produced a classification accuracy of 94.20 %. Subsequently, ten distinct SVM ensemble configurations were investigated. Combining SVM with Light GBM and GBM both resulted in an identical improvement in accuracy to 96.95 %, representing a 2.75 % increase compared to standalone SVM. Among the boosting algorithms, the SVM with the Cat Boost combination yielded the

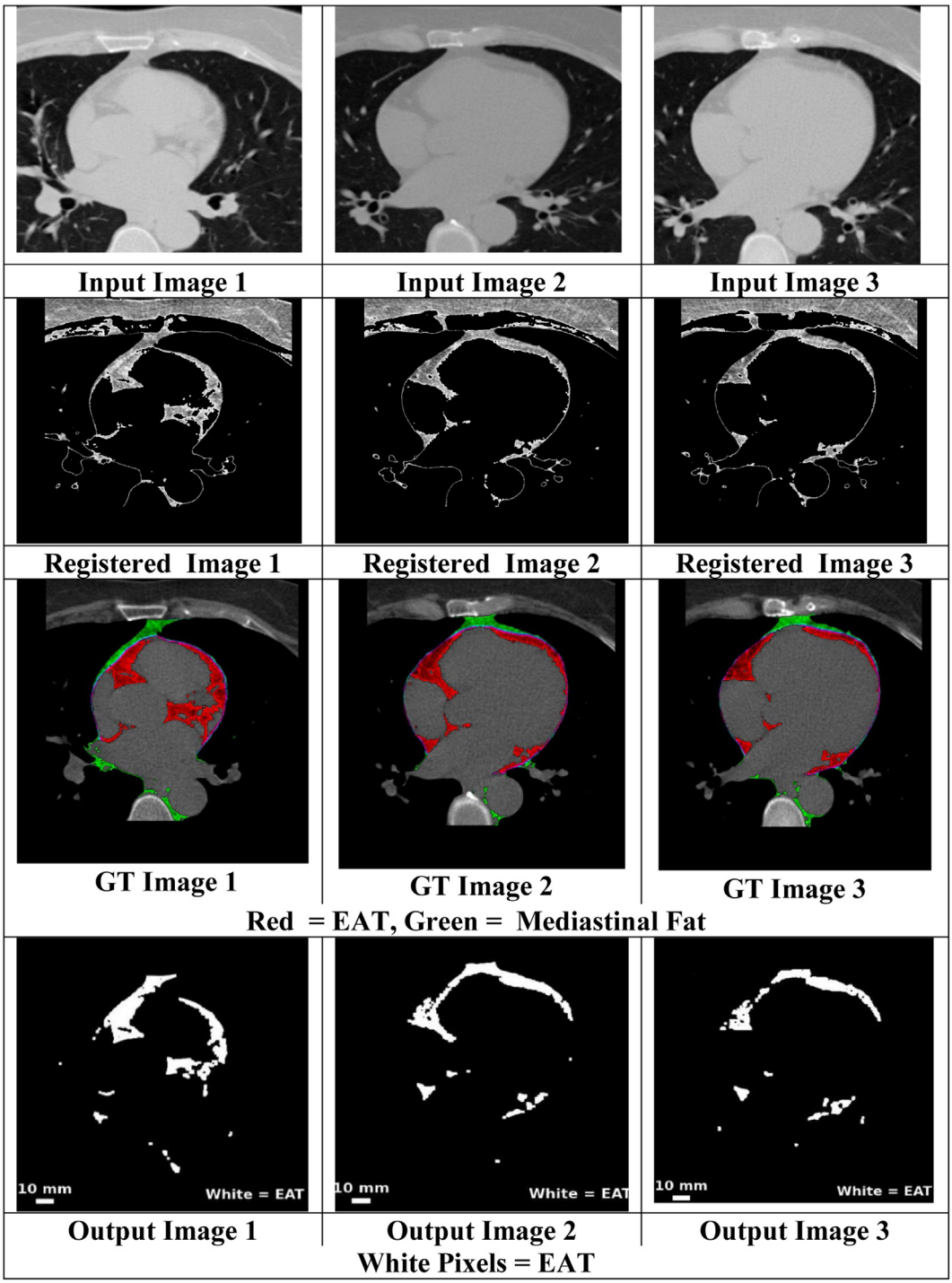

Fig. 5. The samples of (a)The input cardiac CT image, (b) Pre-processed cardiac CT image (c)The Labelled ground truth cardiac CT image, (d)The binary segmented image through the proposed SVM+ANN.

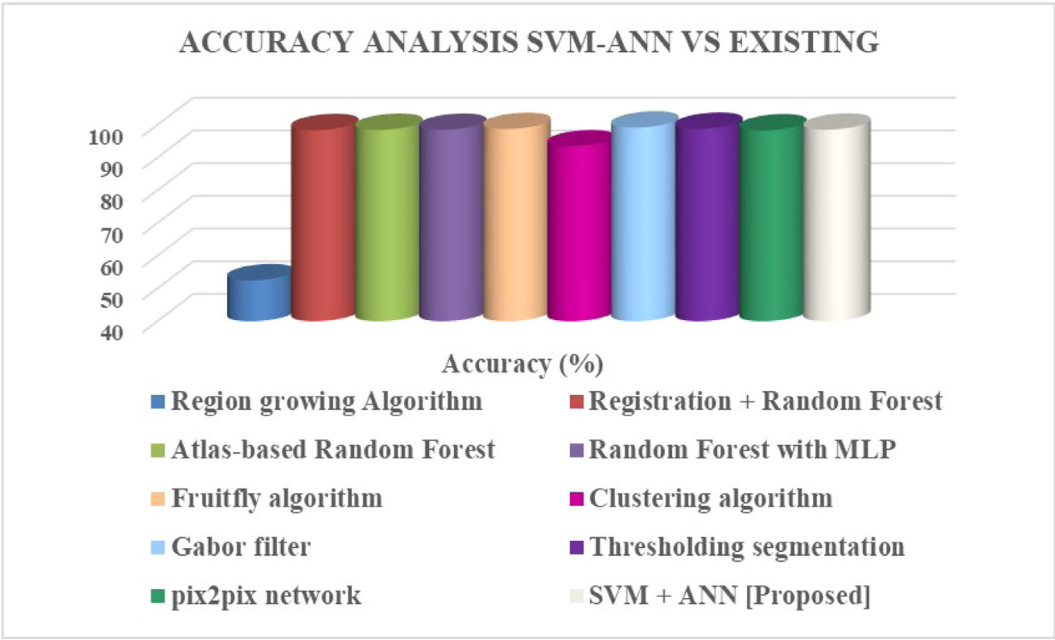

(a)

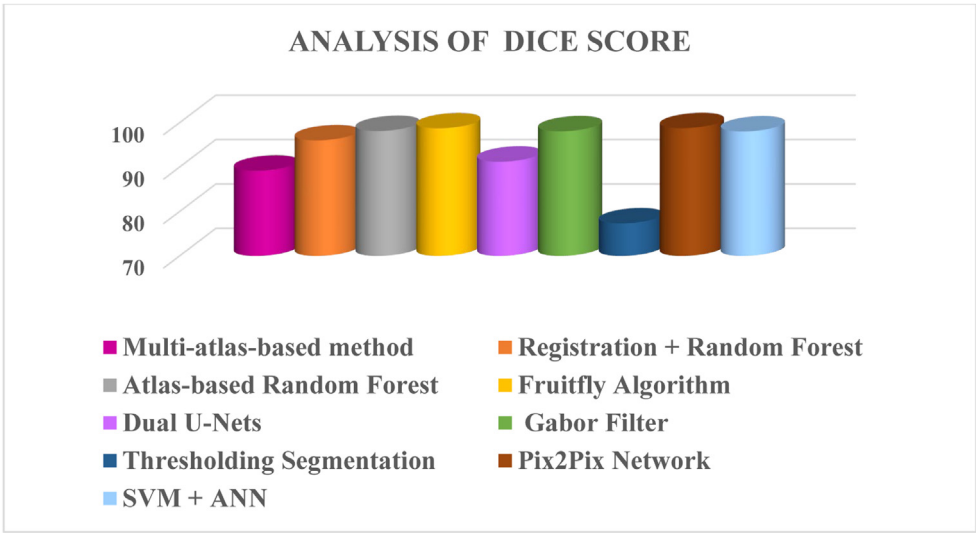

(b)

Fig. 6. Comparative analysis of the SVM-ANN ensemble with existing techniques (a) Analysis of accuracy (b) Analysis of Dice score.

highest accuracy of 97.085 %. When SVM is combined with Random Forest, the accuracy increases to 98.13 %. It is also noted that the accuracy increases to 97.84 % when the SVM with Random Forest combination is integrated with Cat Boost. The SVM with ANN performed better than the other ensemble models, with a Dice score of 98 %, an accuracy of 98.57 %. This ensemble represents an improvement of 4.37 % compared to the standalone SVM. A noteworthy observation is that all ensemble configurations yield higher accuracy compared to the standalone SVM. The outcomes of ten distinct ensemble ML strategies are demonstrated in Table 3, which indicates that the optimal results are achieved through the integration of the SVM with ANN.

Overall, SVM+ANN ensemble demonstrates an improvement in accuracy ranging from 0.44 % to 4.37 %, while the DSC improvement falls within the range of 0.30 % to 3.7 % compared to other ensemble models. The segmentation outcomes of this optimal combination are illustrated in Fig. 5.

Performance comparison of SVM+ANN combination with existing methods

Table 4 details the techniques that are reported in the literature for epicardial fatty tissue delineation using cardiac CT images and compares them to the proposed better-performing SVM with the ANN ensemble technique. The SVM with ANN model demonstrates a high accuracy of 98.57 %, making it highly competitive among the listed models for epicardial fat segmentation. This ensemble combination is only 0.63 % less accurate than cardiac fat segmentation using the Gabor filter, yet it is approximately 42.85 times faster, with a negligible difference in the Dice score. Although the adaptive fruitfly algorithm achieves a marginally higher accuracy of 0.19 %, the SVM with an ANN combination is about 5.35 times faster.

While the pix2pix network is the fastest among existing models, segmenting a cardiac CT image in just 1.44 s, the proposed SVM with the ANN method surpasses this speed by being approximately 1.02 times faster. On the other hand, the 3D U-Net model reported a significantly lower Dice score of 70.97 and required 6 s per image for classification, making it approximately 4.3 times slower than the SVM with ANN ensemble.

The SVM with ANN model provides balanced and robust performance with high accuracy and Dice score and excels in classification speed. This makes it particularly suitable for complex tasks like epicardial fat segmentation. Despite a minor trade-off in accuracy compared to the top-performing model, the significant improvement in speed positions the SVM with the ANN model as an efficient and effective choice among these models. Figs. 6a and 6b provide graphical comparisons of the existing models with the proposed one in terms of accuracy and Dice score, respectively.

Key findings

- The SVM+ANN ensemble achieved 98.57 % accuracy, improving by 4.37 % compared to standalone SVM, which had 94.20 % accuracy.
- The classification time was 1.40 s per image, making it 1.02 times faster than Pix2Pix Network, which required 1.44 s, and 1.028 to 1343.5 times faster than the techniques reported in literature.
- The Gabor filter-based segmentation achieved 99.2 % accuracy, but it was 42.85 times slower, proving the proposed method offers the best balance between accuracy and efficiency.

Advantages of the proposed method

The proposed approach offers several distinct strengths that contribute to its practical utility and technical effectiveness. By combining SVM with MLP through a soft voting mechanism, the method achieves greater classification consistency and improved segmentation accuracy compared to standalone classifiers. The utilization of GLCM texture attributes further refines the model's capacity to distinguish between epicardial fat and other tissues by capturing meaningful spatial patterns that intensity values alone may not reveal.

Importantly, all ten ensemble configurations assessed in this work outperformed the baseline SVM model, underscoring the advantage of incorporating ensemble learning for this application. In contrast to many deep learning-based methods, which often demand extensive computational resources and large annotated datasets, the proposed framework delivers comparable segmentation performance with a notably lower computational burden. Its lightweight structure and fast processing time make it well-suited for integration into real-world clinical workflows, particularly in settings where rapid and reliable analysis is required without access to high-end computing infrastructure.

Limitations

Despite its strong performance, the proposed approach has certain limitations. The dataset size was limited to 20 patients with 878 images, which may affect generalizability. Although ensemble models are designed for robustness, further multi-center validation across diverse populations is required. The manual hyperparameter tuning for SVM and ANN introduces additional computational effort, necessitating optimization techniques. Additionally, the method has only been validated on CT images and requires testing on MRI and ultrasound to confirm its adaptability across different imaging modalities.

Ethics statements

Ethical approval was not required for this study as it used publicly available data, which is fully anonymized and freely accessible.

CRediT author statement

Jasmine: Conceptualisation, Methodology, Software, Writing- Original Draft preparation, Visualisation, Investigation. **Marichamy:** Supervision, Validation, Writing- Reviewing and Editing.

Declaration of competing interest

The authors declare that they have no known competing financial interests or personal relationships that could have appeared to influence the work reported in this paper.

Data availability

The link to the data is provided in the Specifications table.

Acknowledgments

This research is funded by the Tamil Nadu State Council for Science and Technology (Department of Higher Education, Government of Tamil Nadu) under the Programme for Bridging the Gap in Research Funding for Research Scholars in Colleges (RFRS-2022–2023) [TNSCST/RFRS/10/VM/2022-23/16395].

References

[1] A.G. Bertaso, D. Bertol, B.B. Duncan, M. Foppa, Epicardial fat: definition, measurements and systematic review of main outcomes, Arq. Bras. Cardiol. (1) (2013) 101.
[2] N. Alexopoulos, D.S. McLean, M. Janik, C.D. Arepalli, A.E. Stillman, P. Raggi, Epicardial adipose tissue and coronary artery plaque characteristics, Atherosclerosis 210 (1) (2010) 150–154.
[3] Y. Wu, A. Zhang, D.J. Hamilton, T. Deng, Epicardial fat in the maintenance of cardiovascular health, Methodist Debakey Cardiovasc. J. 13 (1) (2017) 20–24.
[4] D. Corradi, R. Maestri, S. Callegari, et al., The ventricular epicardial fat is related to the myocardial mass in normal, ischemic and hypertrophic hearts, Cardiovasc. Pathol. 13 (6) (2004) 313–316, doi:10.1016/j.carpath.2004.08.005.
[5] S. Dabbah, H. Komarov, A. Marmor, N. Assy, Epicardial fat, rather than pericardial fat, is independently associated with diastolic filling in subjects without apparent heart disease, Nutr. Metab. Cardiovasc. Dis. 24 (8) (2014) 877–882.
[6] A.A. Mahabadi, M.H. Berg, N. Lehmann, et al., Association of epicardial fat with cardiovascular risk factors and incident myocardial infarction in the general population: the Heinz Nixdorf Recall Study, J. Am. Coll. Cardiol. 61 (13) (2013) 1388–1395.
[7] C.L. Schlett, M. Ferencik, M.F. Kriegel, et al., Association of pericardial fat and coronary high-risk lesions as determined by cardiac CT, Atherosclerosis 222 (1) (2012) 129–134.
[8] T.E. Brinkley, F.C. Hsu, J.J. Carr, et al., Pericardial fat is associated with carotid stiffness in the Multi-Ethnic Study of Atherosclerosis, Nutr. Metab. Cardiovasc. Dis. 21 (5) (2011) 332 –.
[9] A. Yerramasu, D. Dey, S. Venuraju, et al., Increased volume of epicardial fat is an independent risk factor for accelerated progression of sub-clinical coronary atherosclerosis, Atherosclerosis 220 (1) (2012) 223–230.
[10] R. Djaberi, J.D. Schuijf, J.M. van Werkhoven, G. Nucifora, J.W. Jukema, J.J. Bax, Relation of epicardial adipose tissue to coronary atherosclerosis, Am. J. Cardiol. 102 (12) (2008) 1602–1617.
[11] T.Y. Choi, N. Ahmadi, S. Sourayanezhad, I. Zeb, M.J. Budoff, Relation of vascular stiffness with epicardial and pericardial adipose tissues, and coronary atherosclerosis, Atherosclerosis 229 (1) (2013) 118–123.
[12] P. Mathieu, P. Poirier, P. Pibarot, I. Lemieux, J.P. Després, Visceral obesity: the link among inflammation, hypertension, and cardiovascular disease, Hypertension 53 (4) (2009) 577–584.
[13] I.J. Neeland, C.R. Ayers, A.K. Rohatgi, et al., Associations of visceral and abdominal subcutaneous adipose tissue with markers of cardiac and metabolic risk in obese adults, Obesity (Silver Spring) 21 (9) (2013) E439–E447.
[14] K.A. Britton, J.M. Massaro, J.M. Murabito, B.E. Kreger, U. Hoffmann, C.S. Fox, Body fat distribution, incident cardiovascular disease, cancer, and all-cause mortality, J. Am. Coll. Cardiol. 62 (10) (2013) 921–925.
[15] A. Tchernof, J.P. Després, Pathophysiology of human visceral obesity: an update, Physiol. Rev. 93 (1) (2013) 359–404.
[16] H.S. Sacks, J.N. Fain, Human epicardial adipose tissue: a review, Am. Heart J. 153 (6) (2007) 907–917.
[17] A.A. Mahabadi, N. Lehmann, H. Kälsch, et al., Association of epicardial adipose tissue with progression of coronary artery calcification is more pronounced in the early phase of atherosclerosis: results from the Heinz Nixdorf recall study, JACC Cardiovasc. Imaging 7 (9) (2014) 909–916.
[18] W.T. Chen, J.H. Huang, M.H. Hsieh, Y.J. Chen, Extremely high coronary artery calcium score is associated with a high cancer incidence, Int. J. Cardiol. 155 (3) (2012) 474–475.
[19] K. Dudas, G. Lappas, S. Stewart, A. Rosengren, Trends in out-of-hospital deaths due to coronary heart disease in Sweden (1991 to 2006), Circulation 123 (1) (2011) 46–52.
[20] C.T. Escoffery, S.E. Shirley, Causes of sudden natural death in Jamaica: a medicolegal (coroner's) autopsy study from the University Hospital of the West Indies, Forensic Sci. Int. 129 (2) (2002) 116–121.
[21] R. Sicari, A.M. Sironi, R. Petz, et al., Pericardial rather than epicardial fat is a cardiometabolic risk marker: an MRI vs echo study, J. Am. Soc. Echocardiogr. 24 (10) (2011) 1156–1162.
[22] G. Iacobellis, M.C. Ribaudo, F. Assael, et al., Echocardiographic epicardial adipose tissue is related to anthropometric and clinical parameters of metabolic syndrome: a new indicator of cardiovascular risk, J. Clin. Endocrinol. Metab. 88 (11) (2003) 5163–5168.
[23] T.S. Polonsky, R.L. McClelland, N.W. Jorgensen, et al., Coronary artery calcium score and risk classification for coronary heart disease prediction, JAMA 303 (16) (2010) 1610–1616.
[24] J.Chen H.Hu, W. Shen, Segmentation and quantification of adipose tissue by magnetic resonance imaging, MAGMA 29 (2) (2016) 259–276.
[25] G. Coppini, R. Favilla, P. Marraccini, D. Moroni, G. Pieri, Quantification of epicardial fat by cardiac CT imaging, Open Med. Inform. J. 4 (2010) 126–135.
[26] S.W. Rabkin, Epicardial fat: properties, function and relationship to obesity, Obes. Rev. 8 (3) (2007) 253–261.
[27] G.L. Wheeler, R. Shi, S.R. Beck, et al., Pericardial and visceral adipose tissues measured volumetrically with computed tomography are highly associated in type 2 diabetic families, Invest. Radiol. 40 (2) (2005) 97–101.
[28] D. Dey, Y. Suzuki, S. Suzuki, et al., Automated quantitation of pericardiac fat from noncontrast CT, Invest. Radiol. 43 (2) (2008) 145–153.
[29] É.O. Rodrigues, F.F. Morais, N.A. Morais, L.S. Conci, L.V. Neto, A. Conci, A novel approach for the automated segmentation and volume quantification of cardiac fats on computed tomography, Comput. Methods Programs Biomed. 123 (2016) 109–128.
[30] J.G. Barbosa, B. Figueiredo, N. Bettencourt, J.M. Tavares, Towards automatic quantification of the epicardial fat in non-contrasted CT images, Comput. Methods Biomech. Biomed. Engin. 14 (10) (2011) 905–914.
[31] A.F. Rebelo, A.M. Ferreira, J.M. Fonseca, Automatic epicardial fat segmentation and volume quantification on non-contrast cardiac computed tomography, Comput. Methods Programs Biomed Update. 2 (2022) 100079.
[32] L. Liu, R. Ma, P.M.A. Van Ooijen, M. Oudkerk, R. Vliegenthart, R.N.J. Veldhuis, et al., The U-Net family for epicardial adipose tissue segmentation and quantification in low-dose CT, Technologies 11 (4) (2023) 104.
[33] L. Zhang, J. Sun, B. Jiang, L. Wang, Y. Zhang, X. Xie, Development of artificial intelligence in epicardial and pericoronary adipose tissue imaging: a systematic review, Eur. J. Hybrid Imaging. 5 (1) (2021).

[34] F. Commandeur, P.J. Slomka, M. Goeller, et al., Machine learning to predict the long-term risk of myocardial infarction and cardiac death based on clinical risk, coronary calcium, and epicardial adipose tissue: a prospective study, Cardiovasc. Res. 116 (14) (2020) 2216–2225.
[35] X. He, B.J. Guo, Y. Lei, T. Wang, Y. Fu, W.J. Curran, et al., Automatic segmentation and quantification of epicardial adipose tissue from coronary computed tomography angiography, Phys. Med. Biol. 65 (9) (2020) 095012.
[36] T. Siriapisith, W. Kusakunniran, P. Haddawy, A 3D deep learning approach to epicardial fat segmentation in non-contrast and post-contrast cardiac CT images, PeerJ Comput. Sci. (2021) 7.
[37] R. Shahzad, D. Bos, C. Metz, et al., Automatic quantification of epicardial fat volume on non-enhanced cardiac CT scans using a multi-atlas segmentation approach, Med. Phys. 40 (9) (2013) 091910.
[38] É.O. Rodrigues, A. Conci, F.F. Morais, M.G. Pérez, Towards the automated segmentation of epicardial and mediastinal fats: a multi-manufacturer approach using intersubject registration and random forest, in: 2015 IEEE International Conference on Industrial Technology (ICIT), Seville, Spain, 2015, pp. 1779–1785. *2015 Mar 17–19*.
[39] É.O. Rodrigues, V.H.A. Pinheiro, P. Liatsis, A. Conci, Machine learning in the prediction of cardiac epicardial and mediastinal fat volumes, Comput. Biol. Med. 89 (2017) 520–529.
[40] É.O. Rodrigues, L.O. Rodrigues, L.S.N. Oliveira, A. Conci, P. Liatsis, Automated recognition of the pericardium contour on processed CT images using genetic algorithms, Comput. Biol. Med. 87 (2017) 38–45.
[41] É.O. Rodrigues, F.F. Cordeiro de Morais, A. Conci, On the automated segmentation of epicardial and mediastinal cardiac adipose tissues using classification algorithms, Stud. Health Technol. Inform. 216 (2015) 726–730.
[42] V.H.C. de Albuquerque, D.A. Rodrigues, R.F. Ivo, et al., Fast fully automatic heart fat segmentation in computed tomography datasets, Comput. Med. Imaging Graph. 80 (2020) 101674.
[43] A. Kazemi, A. Keshtkar, S. Rashidi, N. Aslanabadi, B. Khodadad, M. Esmaeili, Correlation between heart mediastinal and epicardial fat volumes and coronary artery disease based on computed tomography images, Iran Heart J (3) (2021) 22.
[44] C. Priya, S. Sudha, Adaptive Fruitfly based modified region growing algorithm for cardiac fat segmentation using optimal neural network, J. Med. Syst. 43 (5) (2019) 104 Published 2019 Mar 15.
[45] A.N. Bandekar, M. Naghavi, I.A. Kakadiaris, Automated pericardial fat quantification in CT data, Conf. Proc. IEEE Eng. Med. Biol. Soc. 2006 (2006) 932–935.
[46] Q. Zhang, J. Zhou, B. Zhang, W. Jia, E. Wu, Automatic epicardial fat segmentation and quantification of CT scans using dual U-Nets with a morphological processing layer, IEEE Access 8 (2020) 128032–128041.
[47] G.S. Da Silva, D. Casanova, J.T. Oliva, É.O. Rodrigues, Cardiac fat segmentation using computed tomography and an image-to-image conditional generative adversarial neural network, Med. Eng. Phys. 124 (2024) 104104.
[48] Y. Wang, A. Wang, L. Wang, W. Tan, L. Xu, J. Wang, S. Li, J. Liu, Y. Sun, B. Yang, S. Greenwald, Automated pericardium segmentation and epicardial adipose tissue quantification from computed tomography images, Biomed. Signal Process. Control 100 (2025) 107167.
[49] L. Liu, R. Ma, P.M.A. van Ooijen, M. Oudkerk, R. Vliegenthart, R.N.J. Veldhuis, C. Brune, The U-Net family for epicardial adipose tissue segmentation and quantification in low-dose CT, Technologies 11 (4) (2023) 1–18.
[50] S. Jasmine, P. Marichamy, Dynamic RU-Next: advancing liver and tumor segmentation with enhanced deep learning architecture, J. Radiat. Res. Appl. Sci. 17 (4) (2024) 101182.
[51] S. Jasmine, P. Marichamy, MNR^{2}NeXt-50: segmentation and quantification of epicardial fat from cardiac CT images using transfer learning with an optimized ensemble model, J. Radiat. Res. Appl. Sci. 18 (3) (2025) 101648.